Characteristic regimes of subgrid-scale coupling in LES of particle-laden turbulent flows

By J. Urzay, M. Bassenne, G. I. Park AND P. Moin

1. Motivation and objectives

Large-Eddy Simulations (LES) of turbulent flows are fundamentally based on resolving eddy sizes larger than a filter width Δ while modeling the subfilter scales. In practice, Δ is imposed by the grid resolution and is ideally representative of scales associated with the inertial subrange. Dynamic subgrid-scale (SGS) models for turbulent transport of momentum and energy have produced relatively accurate computation of single-phase flows at high Reynolds numbers (Moin *et al.* 1991). In LES of particle-laden turbulent flows, however, additional difficulties arise when SGS modeling is pursued, in that closure models are required for the simultaneous description of both phases, including consideration of one-way and two-way coupling effects (Balachandar & Eaton 2010; Sánchez *et al.* 2015).

In most practical applications, difficulties related to SGS modeling of particle-laden flows pertain not only to the effects of unresolved carrier-phase momentum and thermal-energy transport on particle dynamics, as in a one-way coupled direction, but also to the two-way coupled influences that the unresolved particle dynamics have on the carrier phase. While the unresolved one-way coupled interactions in LES involve the repercussion of the missing small scales on particle dynamics, the corresponding two-way coupling phenomena effects are associated with consequences of subgrid energy transfer from the particles to the carrier phase. As described below, the importance of these processes in LES can be described in terms of a reduced number of fundamental dimensionless parameters that account for cutoff scales.

The remainder of this report is structured as follows. Section 2 is focused on describing a set of characteristic scales specific to particle-laden turbulent flows that give rise to different inter-phase SGS-coupling regimes in LES. Additionally, sample numerical computations are performed in Section 3 to investigate the effects of neglecting SGS dynamics on dispersion and preferential concentration of particles in a homogeneous isotropic turbulent flow. Finally, conclusions are drawn in Section 4.

2. Characteristic scales and inter-phase SGS-coupling regimes

In describing the dynamics of particle-laden turbulent flows, it is expedient to consider three characteristic length scales, namely, the particle radius a, the large-scale eddy size ℓ, and the Kolmogorov length ℓ_k, as depicted in Figure 1. The ratio of large-to-small eddy sizes is large in turbulent flows according to the universal-equilibrium scaling $\ell/\ell_k \sim \mathrm{Re}_\ell^{3/4} \gg 1$ obtained from the invariance of the turbulent dissipation $\epsilon \sim u_\ell^3/\ell$ through the inertial subrange of the kinetic-energy cascade. In this formulation, $\mathrm{Re}_\ell = u_\ell \ell/\nu \gg 1$ is a sufficiently large turbulent Reynolds number that warrants separation of scales in the carrier phase, and is based on the large-scale turnover velocity u_ℓ and on the fluid kinematic viscosity ν. In addition to these scales, the filter width Δ, which is imposed by

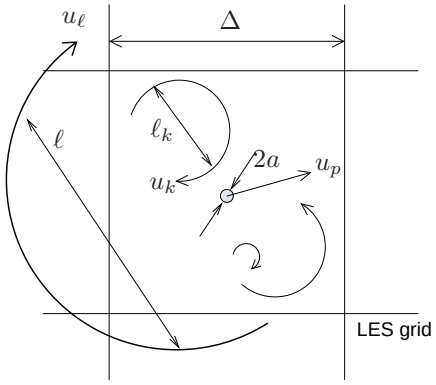

FIGURE 1. Sketch of the model problem.

the grid spacing, plays an important role in LES by delimiting the smallest characteristic length of the resolved turbulence structures.

In most practical applications, the density ρ_p of the particle material is much larger than the carrier-phase density ρ. In gases, the corresponding ratio ρ_p/ρ becomes increasingly larger with decreasing pressure and increasing temperature. For instance, in the subcritical combustion of sprays of typical hydrocarbon liquid fuels, the droplet-to-gas density ratio is of order $\rho_p/\rho \sim 10^2 - 10^3$. Similarly, in flows laden with solid particles of ceramic materials or heavy metals, of interest for particle-based solar receivers, larger values of order $\rho_p/\rho \sim 10^3 - 10^4$ are commonly encountered. That the density ratio ρ_p/ρ is a large parameter is relevant for the separation of fast dynamics at particle scales from slower transport processes developing at larger scales in the carrier phase, as described below.

Two types of SGS inter-phase coupling effects emerge in LES of particle-laden flows. First, the unresolved dynamics of the carrier phase can influence the particles during their flight time in a one-way coupled direction. Additionally, and under sufficiently large mass loading, the energy transferred from the particles to the fluid may cause considerable two-way coupling effects in unresolved scales, including variations of SGS momentum that may lead to turbulence modulation. A description of these two phenomena, along with the associated spatio-temporal scales, is given below.

2.1. *One-way SGS inter-phase coupling regimes*

Restriction is first made in the analysis to small particles compared with Kolmogorov scales, $a/\ell_k \ll 1$, with brief references to the more involved case $a \sim \ell_k$ being deferred to later in the text. In the small-particle limit, the description is greatly simplified when molecular transport prevails over the relative flow advection, thereby making the particle Reynolds number

$$\mathrm{Re}_p = [(u_i - u_{p,i})(u_i - u_{p,i})]^{1/2}\, a/\nu \tag{2.1}$$

a small quantity compared to unity, and the equation of motion of the particle becomes

$$\frac{4}{3}\pi\rho_p a^3 \frac{du_{p,i}}{dt} = 6\pi\mu a(u_i - u_{p,i}), \tag{2.2}$$

with μ being the dynamic viscosity of the fluid. In this formulation, u_i and $u_{p,i}$ denote, respectively, the gas and particle velocity components, with $u_i - u_{p,i}$ a velocity slip that

depends on particle inertia and on the fluctuation time scale of the gas velocity field, as described below.

A number of higher-order corrections to Eq. (2.2) exist (Maxey & Riley 1983). In principle, curvature of the fluid velocity far from the particle can be accounted for in a Faxén correction of order a^2/ℓ_k^2. Similarly, unsteady forces related to virtual-mass displacement and Basset history effects result in additional terms of order ρ/ρ_p and $(\rho/\rho_p)^{1/2}$, respectively, that become vanishingly small at the high density ratios $\rho_p/\rho \gg 1$ considered here. Additionally, fluid-inertia effects at fast relative motion can be quantified in Eq. (2.2) by accounting for a Saffman side force of order $(a/\ell_k)\mathrm{Re}_p$ (Saffman 1965), and by considering an Oseen correction of order Re_p for the drag (Oseen 1910).

In absence of the aforementioned second-order effects, Eq. (2.2) describes a characteristic relaxation of the particle velocity to the local velocity of the fluid in an acceleration time scale of order $t_a \sim (2/9)(a^2/\nu)(\rho_p/\rho)$. Because of the large density ratio, t_a is typically much larger than the characteristic diffusion time a^2/ν. As a result, the dynamics around the particle can be treated quasi-steadily due to the prevailing molecular diffusion at $\mathrm{Re}_p \ll 1$, which enables a separation of slow large-scale transport in the gas environment from the propagation of fast viscous disturbances in the vicinity of the particle. The magnitude of the acceleration time scale t_a, however, is not restricted, and in principle can be comparable to the characteristic hydrodynamic time depending on the specific problem conditions.

In turbulent flows, the fluid velocity u_i in Eq. (2.2) undergoes intermittent variations in time and space with values ranging from the turnover velocity of the large eddies u_ℓ, to the Kolmogorov velocity $u_k \sim u_\ell \mathrm{Re}_\ell^{-1/4} \ll u_\ell$. Nonetheless, some of these fluctuations lie in the subgrid and are not resolved in LES, in which the solution to the filtered conservation equations only provides the resolved fluid velocity $\widetilde{u}_i$. A closure problem not present in single-phase flows therefore arises in Eq. (2.2) in connection with modeling the unresolved one-way coupling effects of SGS fluid-velocity fluctuations $u_i'' = u_i - \widetilde{u}_i$ on the particle motion.

It should be stressed here, however, that their non-zero inertia makes the particles insensitive to a range of SGS fluctuations, which in most instances pertain to the disturbances caused by rapidly turning, low kinetic-energy eddies. In particular, the description of particle motion in turbulent flows largely depends on the relative magnitude of the acceleration time scale t_a in comparison with the turnover time of the eddies $t_n = \ell_n/u_n$. The ratio of those two quantities defines the scale-dependent Stokes number

$$\mathrm{St}_n = t_a/t_n, \tag{2.3}$$

with the restriction $\mathrm{St}_n \ll 1$ determining the size range of the eddies for which the particles behave as tracers. This can be understood by examining the low-pass filtering involved in computing the particle velocity from Eq. (2.2), which can be illustrated in the following manner. Consider a particle released at $t = 0$ with speed u_p^0 in a locally uniform, fluctuating velocity field $u_n = U_n \exp(2\pi j t/t_n)$ of slowly varying amplitude U_n and zero mean, which serve to illustrate, in a simplified way, the effect a single velocity disturbance on the particle motion. In these variables, the component-wise solution to Eq. (2.2) yields the relative velocity

$$u_n - u_p = \frac{2\pi j \mathrm{St}_n u_n}{1 + 2\pi j \mathrm{St}_n} - \left(u_p^0 - \frac{U_n}{1 + 2\pi j \mathrm{St}_n} \right) \exp(-t/t_a), \tag{2.4}$$

where the exponential transient term, which carries information of the initial condition, vanishes after sufficiently long integration periods $t \gg t_a$ along the particle trajectory.

It is worth discussing the implications of Eq. (2.4). As indicated above, the Stokes number St_n determines the sensitivity of the particle motion to aerodynamic fluctuations with time scale t_n. Specifically, for $\mathrm{St}_n \gg 1$ and short integration times $t \ll t_a$, the particle initial motion has not yet been modified by the fluctuating velocity field u_n. As a result, the particle velocity remains close to its initial value $u_p \sim u_p^0$, and the particle Reynolds number $\mathrm{Re}_p \sim (u_n - u_p^0)a/\nu$ is determined by the initial relative slip. At long times $t \gg t_a$, the exponential transient term in Eq. (2.4) disappears and the particle velocity settles to a zero-mean velocity that oscillates out of phase with a vanishing amplitude of order $1/\mathrm{St}_n \ll 1$ relative to the fluid velocity. In this limit, the particle is mostly insensitive to the velocity fluctuation u_n, which causes relative velocities and particle Reynolds numbers of order u_n and $\mathrm{Re}_p \sim u_n a/\nu$, respectively. On the other hand, for $\mathrm{St}_n \ll 1$ soon after deployment the particle follows the fluid with vanishing relative velocities, $u_p - u_n \sim u_n \mathrm{St}_n \ll u_n$, in a regime that yields characteristic particle Reynolds numbers of order $\mathrm{Re}_p \sim (u_n a/\nu)\mathrm{St}_n$. In conclusion, Eq. (2.4) indicates that the relative velocity $u_n - u_p$, along with the corresponding particle Reynolds number (2.1), decrease with decreasing St_n, while the fluid-to-particle velocity transfer function $u_p/u_n = 1/(1 + 2\pi j \mathrm{St}_n)$ decays in frequency space as a first-order low-pass filter with a smooth cutoff Stokes number of order unity, $\mathrm{St}_n = O(1)$.

Despite the information provided by Eq. (2.4), the interaction of particles with turbulent flows is a significantly more complicated phenomenon that is difficult to represent in such a simplified manner. For instance, at high Reynolds numbers the fluid velocity is a broadband field characterized by a wide range of spatio-temporal scales. As a result, for a given particle acceleration time t_a, the Stokes number (2.3) increases with decreasing eddy sizes, with

$$\mathrm{St}_\ell = t_a/t_\ell \tag{2.5}$$

being a characteristic minimum value of St_n based on the turnover dynamics of the large eddies, and

$$\mathrm{St}_k = t_a/t_k \sim \mathrm{St}_\ell \mathrm{Re}_\ell^{1/2} \gg \mathrm{St}_\ell \tag{2.6}$$

corresponding to a maximum value based on the Kolmogorov scales that is not approachable in LES, since such small eddies are beyond the grid resolution.

The characteristic scale of turbulence for which the local Stokes number is of order unity plays an important role in the dynamics of the particles. To see this, consider the first term on the right hand side of Eq. (2.4), which represents the quasi-steady response of the particle slip velocity in a single, zero-mean fluid-velocity disturbance. Since the Stokes number of the particle increases with decreasing eddy turnover times as $1/t_n$, and since the eddy velocity u_n decreases as $t_n^{1/2}$, the amplitude of the slip velocity in spectral space decays for both large and small eddies as $u - u_p \sim c_1 \epsilon^{1/2} \omega^{1/2} t_a$ and $u - u_p \sim c_2 \epsilon^{1/2} \omega^{-1/2}$, respectively, with c_1 and c_2 two numerical constants. Additionally, the maximum slip velocity predicted by Eq. (2.4),

$$u - u_p \sim (\epsilon t_a)^{1/2}, \tag{2.7}$$

is caused by eddy sizes of order

$$\ell_a \sim (\epsilon t_a^3)^{1/2}, \tag{2.8}$$

for which the Stokes number is of order unity, $\mathrm{St}_n = O(1)$.

To characterize the effects of subgrid eddies on particle motion, it is convenient to

define a SGS Stokes number

$$\mathrm{St}_{\mathrm{SGS}} = t_a/t_\Delta \sim \mathrm{St}_k(\ell_k/\Delta)^{2/3} \sim \mathrm{St}_\ell(\ell/\Delta)^{2/3} \tag{2.9}$$

based on the cutoff time scale

$$t_\Delta \sim (\Delta^2/\epsilon)^{1/3}. \tag{2.10}$$

Specifically, $\mathrm{St}_{\mathrm{SGS}}$ corresponds to an intermediate value of the Stokes number that departs from St_ℓ and St_k by factors that depend on the size of the filter relative to ℓ and ℓ_k, respectively.

Consideration of Eqs. (2.4) and (2.9) indicates that the particles are SGS-non-inertial with respect to subgrid eddies when $\mathrm{St}_{\mathrm{SGS}} \ll 1$, in that the particles become sensitive to the high-frequency fluctuations of the turbulence in the subgrid while behaving as tracers for the large eddies. In this limit, a model for the SGS fluid-velocity fluctuations is required in Eq. (2.2) to account for the effects of the unresolved scales. This limit, for instance, is attained in conditions of interest for solar-power receivers based on distributed absorption of heat by particles in the bulk of the co-flowing air, for which the particles are sufficiently small to render order-unity Kolmogorov-based Stokes numbers $\mathrm{St}_k = O(1)$ and correspondingly small integral-based Stokes numbers $\mathrm{St}_\ell \sim \mathrm{Re}_\ell^{-1/2} \ll 1$. As a consequence, the particles slip predominantly on the small eddies while following the motion of the large scales. This phenomenon results in small particle Reynolds numbers, $\mathrm{Re}_p \sim u_k a/\nu \sim a/\ell_k \ll 1$, for which the viscosity-dominated Stokes region extends to distances of order ℓ_k away from the particle surface. The resulting slip velocities $u - u_p \sim u_k - u_p = O(u_k)$ amount to small fractions of the large-scale turnover velocity u_ℓ. Existing SGS models in this regime involve, for instance, the use of approximate deconvolution methods (Kuerten 2006), stochastic differential equations (Fede *et al.* 2006; Jin & He 2013; Gorokhovski & Zamansky 2014; Mazzitelli *et al.* 2014) and hybrid methods that mix both of those approaches (Michaek *et al.* 2014).

In the opposite limit, $\mathrm{St}_{\mathrm{SGS}} \gg 1$, the particles become ballistic or SGS-inertial with respect to subgrid eddies, and the resolved fluid velocity $\widetilde{u}_i$ suffices to describe the particle motion in Eq. (2.2) with no additional subgrid modeling being required in the one-way coupled formulation. This, for instance, is the relevant limit for droplet dispersion in most spray-combustion applications, in that atomizers are typically designed to break liquid filaments into droplets whose acceleration times (which are comparable to the droplet vaporization times) are similar to the time scales of the large-scale turbulence in the combustor, thereby warranting full penetration of the fuel spray into the air environment. In these conditions, order-unity integral-based Stokes numbers $\mathrm{St}_\ell = O(1)$ are encountered. As a result, the relative motion is mostly dominated by the slippage on the large eddies, $u - u_p \sim u_\ell - u_p = O(u_\ell)$, with characteristic droplet Reynolds numbers of order $\mathrm{Re}_p \sim u_\ell a/\nu$ being determined by the integral scales of the turbulence.

Because of the large density ratio considered, $\rho_p/\rho \sim 10^2 - 10^4$, the small-particle approximation $a/\ell_k \ll 1$ is expected to remain valid in most of the dynamical range of interest, with exceptions found in flows at sufficiently large Reynolds numbers. Specifically, only at exceedingly large Kolmogorov-based Stokes numbers $\mathrm{St}_k \sim \rho_p/\rho \gg 1$ the particle size becomes comparable to the Kolmogorov length, $a \sim \ell_k$. In this limit, and unless the Reynolds number of the turbulence Re_ℓ is larger than a quantity of order $(\rho_p/\rho)^2$, the finite size of the particles leads to SGS-inertial conditions and impractically large values of the integral-based Stokes number, $\mathrm{St}_\ell \sim (\rho_p/\rho)\mathrm{Re}_\ell^{-1/2} \gg 1$, as observed from Eq. (2.6). This, however, is a case of limited interest for studies of turbulence-

enhanced dispersion of particles, since their motion would exclusively be conditioned by their initial velocities.

One-way coupled interactions of finite-size particles ($a \sim \ell_k$) with large-scale turbulence arise at large Reynolds numbers, $\mathrm{Re}_\ell \gtrsim (\rho_p/\rho)^2$, for which the integral-based Stokes number becomes of order unity or smaller. The representative particle Reynolds number in that situation is moderately large and of order $\mathrm{Re}_p \sim (\rho_p/\rho)^{1/2}$, as obtained by considering slip velocities of order u_ℓ. This regime requires revision of the Stokes drag in Eq. (2.2) to account for fluid inertia in conjunction with possibly additional effects related to the presence of velocity gradients at particle scales. However, in this regime the particles are SGS-inertial or ballistic with respect to the subgrid eddies, with the corresponding SGS Stokes number being larger than unity by a factor of order $(\ell/\Delta)^2$ that depends on the relative value of the filter width with respect to the integral length scale, thereby suggesting that in principle the resolved fluid velocity field suffices to describe the particle trajectories.

Effects of subgrid turbulence on the dynamics of finite-size particles ($a \sim \ell_k$) become important at larger Reynolds numbers of order $\mathrm{Re}_\ell \sim (\ell/\Delta)^{4/3}(\rho_p/\rho)^2$ and above, which enable regimes of small SGS Stokes numbers $\mathrm{St}_{\mathrm{SGS}} \lesssim 1$ in a range of SGS-non-inertiality that requires, besides modification of Eq. (2.2) to account for finite Re_p as described above, subgrid modeling of fluid-velocity fluctuations for computing the particle motion. Under these conditions, the large separation of scales in the turbulent flow makes the particles small compared with the filter width, the corresponding ratio of those two quantities being of order $a/\Delta \sim \ell_k/\Delta \sim (\rho_p/\rho)^{-1/2} \ll 1$ and smaller.

An analogous description of SGS inertial and non-inertial regimes can be given to address the effects of SGS temperature fluctuations when considering inter-phase heat transfer in non-isothermal particle-laden flows. In addition to small particle Reynolds numbers $\mathrm{Re}_p \ll 1$, here the approximation requires much higher thermal conductivities in the particle than in the fluid, a requirement that is met by many dispersed phases of practical interest. In this limit, the spherico-symmetrical solution of the heat equation around the particle, subject to the fluid temperature T at infinity and to the uniform particle temperature T_p on its surface, leads to the energy balance

$$\frac{4}{3}\pi\rho_p c a^3 \frac{dT_p}{dt} = 4\pi\kappa a(T - T_p), \tag{2.11}$$

where c is the particle specific heat and κ is the fluid thermal conductivity. A thermal relaxation time $t_q \sim (3/2)(c/c_p)\mathrm{Pr}\, t_a$ can be inferred from Eq. (2.11), with Pr and c_p being, respectively, the Prandtl number and the constant-pressure specific heat of the fluid. However, t_q is typically of the same order as the acceleration time scale t_a since the specific heat ratio c/c_p and the Prandtl number are order-unity parameters in most conditions. Therefore, the thermal Stokes number of the particles resembles the kinematic Stokes number (2.3) up to an order-unity multiplicative factor that has no relevance in the scaling analysis, and the discussion of thermal coupling parallels that of momentum coupling.

2.2. *Two-way SGS inter-phase coupling regimes*

The importance of the effects of the dispersed phase on the carrier fluid is measured by the mass-loading ratio

$$\alpha = (4/3)\pi a^3 \rho_p n/\rho, \tag{2.12}$$

defined as the mass of particles per unit mass of surrounding fluid, with n being a characteristic number density of particles that can be associated with an inter-particle distance $\delta_p \sim n^{-1/3}$. For $\alpha \ll 1$, the dilution in the particle cloud is too large to cause any statistical modification of momentum in the carrier phase. By way of contrast, the two-way inter-phase coupling is most effective for $\alpha = O(1)$, in that the balance

$$\rho \frac{\mathrm{D}u_i}{\mathrm{D}t} \sim 6\pi\mu a n(u_{p,i} - u_i) \tag{2.13}$$

is reached between the convective transport of momentum in the fluid and the collective force per unit volume exerted by the particle cloud, with particles gaining or draining energy predominantly from eddies whose Stokes number is of order unity, $\mathrm{St}_n = O(1)$, as suggested by the discussion in the previous section. Additionally, increasing the mass loading ratio leads to increasingly large influences of the extra viscous dissipation $\rho\epsilon_p = 6\pi\mu a n(u_{p,i} - u_i)(u_{p,i} - u_i)$ produced by the collective effect of the shear due to the non-slip boundary conditions on the particle surfaces, which becomes of the same order as the turbulent dissipation per unit volume $\rho\epsilon$ when $\alpha = O(1)$, as indicated by the approximation $\epsilon_p \sim 6\pi\mu a n \epsilon t_a$ obtained by making use of Eq. (2.7).

At the high density ratios considered here, $\alpha = O(1)$ implies large mean inter-particle distances compared with the particle radius, $\delta_p/a \sim (\rho_p/\rho)^{1/3} \sim 10 - 20$, and correspondingly small volume fractions $\phi \sim \rho/\rho_p \sim 10^{-3} - 10^{-4}$. Particle-particle interactions correspond to second-order effects except in regions of preferentially concentrated particles where departures from these mean estimates may occur.

Depending on the SGS Stokes number, the two-way coupling effects in LES may be more intense in the subgrid than in resolved field. To quantify the relative resolution of these effects, the SGS Stokes number (2.9) is recast in the form

$$\mathrm{St}_{\mathrm{SGS}} = (\ell_a/\Delta)^{2/3}, \tag{2.14}$$

where use has been made of Eqs. (2.8) and (2.10). The Stokes number (2.14) is indicative of whether the preferentially coupled scale is resolved or, conversely, lies in the subgrid. In particular, the subgrid is unloaded when $\alpha = O(1)$ and $\mathrm{St}_{\mathrm{SGS}} \gg 1$, in that the particles are SGS-inertial with respect to the subgrid eddies and coupling is most effective with respect to the resolved scales. On the other hand, the subgrid is loaded for $\alpha = O(1)$ and $\mathrm{St}_{\mathrm{SGS}} \ll 1$, with SGS-non-inertial particles coupling preferentially with subgrid eddies while behaving as tracers for the resolved scales. The two-way coupling effects are, however, much less intense in the SGS-loaded case than in the SGS-unloaded one, in that particle slippage occurs predominantly on large eddies in SGS-unloaded flows under correspondingly larger turbulence modulation. However, the SGS-loaded case requires additional modeling of the fluid-velocity subgrid fluctuations in computing the transfer of energy from the particles to the fluid.

Inter-phase coupling of momentum invariably requires inter-phase coupling of energy and vice-versa, unless unusually large departures from unity occur in the thermal-capacity ratio c/c_p as described above. In this way, $\alpha = O(1)$ enables order-unity thermal-energy variations in the fluid that are caused by energy exchange with the dispersed phase,

$$\rho c_p \frac{\mathrm{D}T}{\mathrm{D}t} \sim 4\pi\kappa a n(T_p - T), \tag{2.15}$$

with particles predominantly modifying the thermal energy of eddies whose Stokes number is unity. The discussion on two-way coupled thermal-energy transfer therefore parallels that of momentum transfer.

Re_λ	80.0	Taylor-Reynolds number
St_k	1.0	Kolmogorov-based Stokes number
$\mathrm{St}_{\mathrm{SGS}}$	0.1	SGS Stokes number
α	0.0001	mass-loading ratio
Re_p	0.1	particle Reynolds number
ρ_p/ρ	1000	particle-to-gas density ratio
Δ/ℓ_k	2.0	grid spacing to Kolmogorov-length ratio (DNS)
Δ/ℓ_k	18.0	grid spacing to Kolmogorov-length ratio (LES)

TABLE 1. Characteristic dimensionless parameters in the computations.

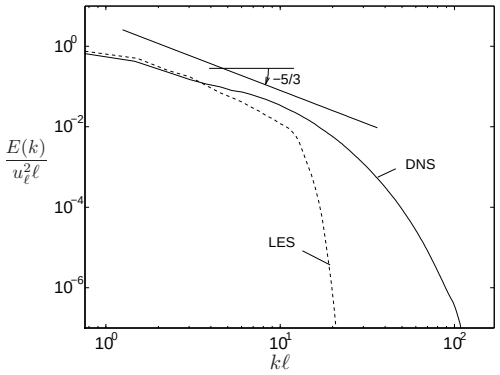

FIGURE 2. Kinetic-energy spectra in LES and DNS.

3. Numerical simulations

In this section, results from numerical simulations of particle-laden forced homogeneous isotropic turbulence are shown for both DNS and LES resolution settings that illustrate the effects of neglecting SGS fluid-velocity fluctuations in Eq. (2.2). The computational parameters are listed in Table 1.

In the computations, homogeneous isotropic turbulent motion was sustained in a triply periodic domain by using linear forcing in physical space. Additional details about the forcing procedure are available elsewhere (Rosales & Meneveau 2005). The computations were first run without particles to allow the turbulence to reach a statistically stationary state. Results were analyzed after 5 integral times had passed since deployment of the particles. The computations were one-way coupled because of the small mass-loading ratios involved. The dynamic model of Moin *et al.* (1991) was used in LES as a closure model for the SGS transport of momentum in the carrier phase.

The numerical method is based on a low-Mach number, central second-order in space, second-order in time, finite-difference scheme that incorporates a Lagrangian set of ordinary-differential equations to compute particle trajectories and velocities (Pouransari *et al.* 2014). The calculations were conducted on a staggered, structured uniform cartesian grid with 256^3 and 32^3 elements in the DNS and LES configurations, respectively. Sample kinetic-energy spectra from the computations are shown in Figure 2 for DNS and LES, with four decades of decay being observed along two decades of wavenumbers in the DNS.

The small SGS Stokes number employed in the simulations renders the particles SGS-non-inertial according to the description given in Section 2, with a subgrid model for the velocity fluctuations being in principle needed for computing the particle motion in Eq. (2.2). The results are analyzed in terms of particle dispersion and particle con-

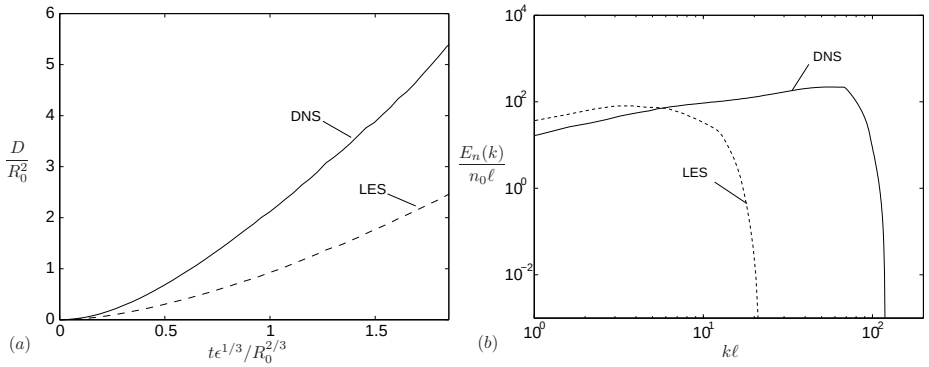

FIGURE 3. LES and DNS results for (a) particle dispersion and (b) particle concentration spectra.

centration, with LES without SGS model for the particles leading to underprediction of dispersion and artificial modification of characteristic lengths associated with regions under preferential-concentration effects.

3.1. *Particle dispersion*

The relative dispersion of two particles, understood as the mean square of the modulus of their separation distance $D = \langle |\delta \mathbf{R}_p|^2 \rangle_{\mathrm{N}_p}$ is a relevant indicator of performance for LES of particle-laden flows. In this formulation, $\delta \mathbf{R}_p = [\mathbf{R}_{p,i} - \mathbf{R}_{p,i}(t=0)] - [\mathbf{R}_{p,j} - \mathbf{R}_{p,j}(t=0)]$ is the relative separation between two particles i and j, with $\mathbf{R}$ the corresponding position vector. Additionally, the angular brackets indicate averaging over all pairs of particles. At $t = 0$, the particles are deployed in local kinematic equilibrium with the gas, in a uniform spatial distribution of inter-particle distance $25\ell_k$ that is representative of the inertial subrange.

Figure 3(a) shows the time evolution of the particle dispersion for both DNS and LES computational settings after sampling 10,000 particles. In a way similar to passive-scalar dispersion, the relative distance between particles computed from DNS grows parabolically in time, with LES showing a deficit of dispersion in amounts of order unity during a single turnover time of a $25\ell_k$-sized eddy. This under-prediction is related to both the absence of SGS model for the particle motion and the alteration of space-time correlations commonly obtained as a result of not resolving the small scales of turbulence (Jin & He 2013).

3.2. *Preferential concentration*

The finite inertia makes the particles to centrifuge away from vortical regions and preferentially concentrate in zones of high strain rates (Robinson 1956). The characteristic spatial scales associated with those accumulation regions can be inferred from wavenumbers corresponding to peaks in the particle-concentration spectra (Jin *et al.* 2010). In Lagrangian formulations, a scalar number-density field n can be computed by combining the discrete position of the particles and using an interpolation or tessellation scheme.

Figure 3(b) shows the volume- and time-averaged spectra of particle-number density for DNS and LES obtained by using a trilinear interpolation among particle coordinates to compute n. While the DNS indicates that the maximum of the concentration spectrum involves wavenumbers corresponding to spatial scales of thin accumulation zones, which are comparable to the thickness of the smallest and most strained turbulent ed-

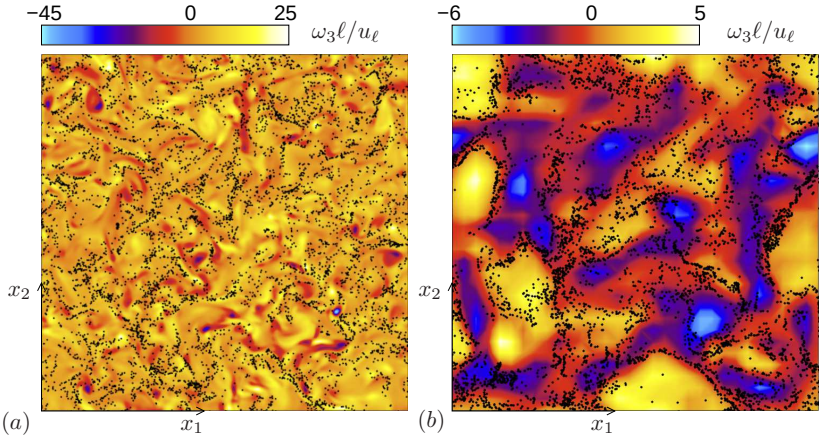

FIGURE 4. Instantaneous spatial distribution of particles (dark dots) overlaid on x_3-vorticity contours in (a) DNS, and (b) LES.

dies, the LES over-predicts the spatial extent of those regions, mainly due to the fact that such thin regions or high wavenumbers are not supported by the LES grid. Alternatively, this can be understood by looking at the instantaneous vorticity contours shown in Figure 4. Specifically, the under-prediction of vorticity and strain-rate in LES leads to thicker turbulent structures that make the particles to preferentially concentrate at smaller wavenumbers with respect to the fine accumulation scales observed in DNS.

4. Concluding remarks

In this study, an analysis of characteristic scales is employed to describe regimes of SGS coupling in LES of particle-laden turbulent flows. Two dimensionless parameters, namely, the SGS Stokes number $\mathrm{St}_{\mathrm{SGS}}$ and the mass-loading ratio α are central to the description. In one-way coupled flows, $\alpha \ll 1$, the interaction of particles with the subgrid eddies involve two different regimes. First, the regime $\mathrm{St}_{\mathrm{SGS}} \gg 1$ corresponds to SGS-inertial particles, which are ballistic with respect to the subgrid eddies. On the other hand, the opposite limit $\mathrm{St}_{\mathrm{SGS}} \ll 1$ represents SGS-non-inertial particles, which behave as tracers for the large eddies but become sensitive to the high-frequency fluctuations of the turbulence in the subgrid, this being a regime that requires consideration of SGS models for particle motion. In two-way coupled flows, $\alpha = O(1)$, the effects of particles on the carrier phase predominantly occur in resolved or unresolved scales when $\mathrm{St}_{\mathrm{SGS}} \gg 1$ and $\mathrm{St}_{\mathrm{SGS}} \ll 1$, respectively, the latter limit requiring SGS modeling of two-way coupled phenomena. For finite-size particles up to diameters comparable to the Kolmogorov length, one-way coupled interactions with SGS turbulence become important only at large Reynolds numbers of the same order as density-ratio squared. However, in two-way coupled flows with $\alpha = O(1)$, the extra viscous dissipation due to finite-size particles becomes of the same order as the turbulent dissipation. Additionally, DNS and LES of particle-laden homogeneous isotropic turbulence at $\mathrm{St}_{\mathrm{SGS}} \ll 1$ are utilized to illustrate the effects of not using SGS modeling for particles on relative dispersion and preferential concentration. Specifically, LES without SGS model for the particles leads to under-prediction of dispersion and artificial widening of characteristic lengths associated with regions under preferential-concentration effects.

Acknowledgments

This investigation is funded by the Advanced Simulation and Computing (ASC) program of the US Department of Energy's National Nuclear Security Administration via the PSAAP-II Center at Stanford.

REFERENCES

Balachandar S. & Eaton J. K. 2010 Turbulent dispersed multiphase flow. *Annu. Rev. Fluid Mech.* **42**, 111–133.

Fede, P., Simonin, O., Villedieu, P. & Squires, K. D. 2006 Stochastic modeling of the turbulent subgrid fluid velocity along inertial particle trajectories. *Proceedings of the Summer Program*, Center for Turbulence Research, Stanford University, pp. 247–258.

Moin, P., Squires, K., Cabot, W. & Lee, S. 1991 A dynamic subgrid-scale model for compressible turbulence and scalar transport. *Phys. Fluids* **3**, 2746–2757.

Gorokhovski, M. & Zamansky R. 2014 Lagrangian simulation of large and small inertial particles in a high Reynolds number flow: Stochastic simulation of subgrid turbulence/particle interactions. *Proceedings of the Summer Program*, Center for Turbulence Research, Stanford University, pp. 37–46.

Jin, G., He, G.W. & Wang L. P. 2010 Large-eddy simulation of turbulent collision of heavy particles in isotropic turbulence. *Phys. Fluids* **22**, 055106.

Jin, G. & He, G.W. 2013 A nonlinear model for the subgrid timescale experienced by heavy particles in large eddy simulation of isotropic turbulence with a stochastic differential equation. *New J. Phys.* **15**, 035011.

Kuerten J. G. M. 2006 Subgrid modeling in particle-laden channel flow. *Phys. Fluids* **18**, 025108.

Maxey M. R. & Riley J. J. 1983 Equation of motion for a small rigid sphere in a nonuniform flow. *Phys. Fluids* **26**, 883–889.

Mazitelli, I. M., Toschi, F. & Lanotte, A. S. 2014 An accurate and efficient Lagrangian sub-grid model. *Phys. Fluids* **26**, 095101.

Michaek, W. R., Kuerten, J. G. M., Zeegers, J. C. H., Liew, R., Pozorski, J. & Geurts, B. J. 2013 A hybrid stochastic-deconvolution model for large-eddy simulation of particle-laden flow. *Phys. Fluids* **25**, 123302.

Oseen, C. W. 1910 Ueber die Stokes'sche Formel, und über eine verwandte Aufgabe in der Hydrodynamik. *Ark. Math. Astronom. Fys.* **6**, 154–155.

Pouransari, H., Kolla, H., Chen J. H. & Mani, A. 2014 Spectral analysis of energy transfer in variable density, radiatively heated particle-laden flows. *Proceedings of the Summer Program*, Center for Turbulence Research, Stanford University, pp. 27–36.

Rosales, C. & Meneveau C. 2005 Linear forcing in numerical simulations of isotropic turbulence: Physical space implementations and convergence properties. *Phys. Fluids* **17**, 095106.

Robinson, A. 1956 On the motion of small particles in a potential field of flow. *Comm. Pure Appl. Math.* **9**, 69–84.

Sánchez, A. L., Urzay, J. & Liñán, A. 2014 The role of separation of scales in the description of spray combustion. *Proc. Comb. Inst.* **35**, 1549–1577.

Saffman, P. G. 1965 The lift on a small sphere in a slow shear flow. *J. Fluid Mech.* **22**, 385–400.